Available online at www.sciencedirect.com

SciVerse ScienceDirect

journal homepage: www.elsevier.com/locate/he

A thermodynamic approach for the development of austenitic steels with a high resistance to hydrogen gas embrittlement

M. Martín, S. Weber, W. Theisen*

Ruhr-Universität Bochum, Institut für Werkstoffe, Lehrstuhl Werkstofftechnik, D-44780 Bochum, Germany

ARTICLE INFO

Article history:
Received 2 May 2013
Received in revised form
6 August 2013
Accepted 29 August 2013
Available online 7 October 2013

Keywords:
Gibbs energy
CALPHAD method
Hydrogen gas embrittlement
Austenite stability
Strain-induced martensite
Alloy development

ABSTRACT

The CALPHAD method was employed to assess the austenite stability of model alloys based on the Cr–Mn–Ni–Cu system. Stability was evaluated as the difference in Gibbs free energy between the austenite and ferrite phases. This energy difference represents the chemical driving force for the martensitic transformation and is employed as a design criterion. Six novel alloys featuring a lower driving force compared to the reference material AISI 316L were produced in laboratory. The susceptibility of all alloys to hydrogen gas embrittlement was evaluated by slow strain-rate tensile testing in air and hydrogen gas at 40 MPa and −50 °C. The mechanical properties and ductility response of four of the six alloys exhibited an equivalent performance in air and hydrogen. Thermodynamic calculations were in agreement with the amount of α'-martensite formed during testing. Furthermore, a 4.5 wt.% reduction in the nickel content in comparison to 316L promises a cost benefit for the novel materials.

1. Introduction

Implementation of a hydrogen economy is limited by the deleterious effect of hydrogen on the mechanical properties of most metallic materials. Since the ductility response is severely reduced by the presence of hydrogen, this phenomenon is usually referred to as hydrogen embrittlement (HE) [1]. If hydrogen arises from a gaseous environment, the resulting interaction is described as hydrogen gas embrittlement (HGE). Currently, high-alloyed austenitic stainless steels, such as AISI types 316 and 310, are selected for hydrogen applications owing to their high resistance to HE [2–7]. Nevertheless, the use of these types of alloys for hydrogen applications is restricted to prototypes or the discontinuous production of parts due to the high costs driven by the high nickel and molybdenum contents. Lowering the amount of nickel in these steel grades led to values ranging between 11.5 mass-% and 13 mass-%, which still results in a drawback concerning cost-efficiency [8–11]. Accordingly, novel alloys with equivalent properties but lower associated costs are needed for mass production of components, e.g. for hydrogen-powered cars.

There are few literature contributions that consider the economic aspects of HE-resistant materials. The systems Fe–22Cr–13Ni–5Mn [12–14], Fe–21Cr–6Ni–9Mn [12,13,15,16] and Fe–0.1C–10Mn–8Ni–2.5Al [17] are examples of such studies. These types of alloys either obey screening tests [12,13] or empirical developments [17]. Both methodologies are quite expensive in terms of time and financial resources. Therefore, the possibility of finding a design criterion to reduce time and expenses is of major interest for alloy

* *Corresponding author*. Tel.: +49 (0234) 3222366; fax: +49 (0234) 3214104.
E-mail address: martin@wtech.rub.de (M. Martín).

0360-3199/$ – see front matter
http://dx.doi.org/10.1016/j.ijhydene.2013.08.133

development. Since the ductility of austenitic steels in hydrogen decreases with increasing volume fraction of strain-induced α'-martensite [2–7,18], the design criterion used in this work was based on the tendency of the material to undergo this phase transformation. Technological features such as the geometry of segregations [9,19], heat treatments [20] and machining operations [21] also play an important role in the material's susceptibility to HGE. Moreover, the deformation mode of the alloy strongly influences the behaviour of the material in hydrogen [16,22,23]. Although all these features contribute to the loss of ductility in hydrogen, minimising the formation of strain-induced martensite has been identified as the first step to overcome in order to increase the resistance against HGE [4,18,24]. Furthermore, although designing a fully stable material does not guarantee a high resistance to HGE [23,25,26], no resistance to HGE can be expected if the alloy behaves in a metastable manner [5,18,26–28].

Based on preliminary investigations, a thermodynamic approach was implemented as a design criterion to define novel chemical compositions by means of computational thermodynamics prior to alloy production. Supported by the CALPHAD method, the driving force behind the martensitic transformation is evaluated as the difference in Gibbs free energy between the austenite and ferrite phases. This is interpreted in terms of austenite stability [29–31].

2. Experimental

2.1. Production of alloys

The novel alloys were produced in the laboratory via ingot casting in a vacuum induction furnace. As-cast ingots with a weight of 3 kg and a diameter of 50 mm were pre-machined to 42 mm and hot-worked in several passes to a final diameter of 16 mm. The as-forged bars were solution-annealed at 1150 °C, followed by water quenching. Tensile specimens with a gauge length of 30 mm and a diameter of 5 mm were produced by means of wet-turning, as described in [21]. The as-turned specimens were heat-treated in an industrial vacuum furnace at 1150 °C for 30 min and quenched with argon at a pressure of 200 kPa to avoid undesirable surface effects [21].

Semi-finished bars of austenitic stainless steel AISI type 316L, provided by Deutsche Edelstahlwerke (DEW, Germany), were employed as the reference material. Tensile specimens were machined out of the centre of 30 mm diameter bars, heat-treated in the same vacuum furnace for 30 min at 1050 °C and quenched with argon.

2.2. Testing

Tensile tests in air and in pure hydrogen gas (≥99.9999% H_2) were carried out at −50 °C with an initial strain rate of $5.5 \cdot 10^{-5}\ s^{-1}$ to account for the effect of temperature and strain rate on HGE susceptibility [27,32–34]. The selected parameters represent a condition of "maximum embrittlement" for most metallic materials [5,10,35,36]. Ambient pressure was used for the air-tested specimens, whereas 40 MPa was used for the tests in a hydrogen atmosphere. For hydrogen testing, the vessel was purged three times with pure nitrogen at 1 MPa, followed by eight consecutive purges with pure hydrogen at 1 MPa before filling to the test pressure. This procedure ensures safety and gas purity. In the hydrogen tests, the load was measured by an internal load cell in all cases. Clip gauge/extensometer measurements were used in air/hydrogen environments to determine the 0.2% proof stress. A total of four tests were performed on every alloy: two in air and two in a hydrogen atmosphere. The measured properties were yield strength ($Rp_{0.2}$), ultimate tensile strength (R_m) and elongation to rupture (A). Additionally, the reduction of area (Z) was obtained *ex situ* by measuring the initial and final diameters of the specimen at the necking circumference with a digital calliper. The Z parameter is known to be very sensitive for qualifying the susceptibility of metallic materials to HGE [5,26,37].

The ferrite equivalent value of every specimen after tensile testing was also obtained *ex situ* by means of a FeritScope® MP30 device (Helmut Fischer GmbH, Germany). This value was obtained as the average of four measurements radially distributed at the midpoint of the uniformly elongated region and represents the amount of material that undergoes a $\gamma \rightarrow \alpha'$ martensitic transformation [38]. Moreover, digital microscopy was implemented to evaluate the fracture surfaces and necking regions of the as-tested specimens at a magnification of 50×. The latter was performed using a VHX-600D digital microscope (Keyence GmbH, Germany).

3. Design criterion and results

3.1. Preliminary results on the thermodynamic stability

The susceptibility of austenitic steels to HGE is frequently related to the stability of the austenitic phase against the α'-martensite transformation [2–5,27,28]. Such stability can be assessed experimentally by empirical formulae or by thermodynamic calculations [5,39,40]. Previous investigations on HGE of modified AISI type 304 steels established a relationship between the loss of ductility in hydrogen and the thermodynamic stability of the austenite phase [26]. Equation (1) was used to evaluate the thermodynamic stability, which represents the chemical driving force for the martensitic transformation [29–31]. The obtained parameter, $\Delta G_{\gamma/\alpha}$, allows a direct comparison of different alloys: the higher the absolute value of $\Delta G_{\gamma/\alpha}$ is, the higher is the chemical driving force available for the martensitic transformation. The results obtained in [26] are summarised in Fig. 1 and are based on the compositions and properties presented in Table 1. Fig. 1 depicts the reduction of area in hydrogen (Z_{H_2}) and the ferrite equivalent fraction in air of three alloys: a low-manganese 304 steel (304_{Mn}), a high-molybdenum 304 steel (304_{Mo}) and a 316L steel [26]. Magnetic response measurements performed *ex-situ* on the uniform elongated area of air-tested tensile specimens showed a marked difference in the corresponding ferrite equivalent fraction (F.E. in Fig. 1). Such values are representative of the material's volume fraction that transforms to martensite upon deformation [17,26,38]. Since the three alloys undergo a uniform elongation of $A_{g-air} \approx 53\%$ (Table 1), an equivalent mechanical driving force for the martensitic transformation is expected in the three materials. Therefore,

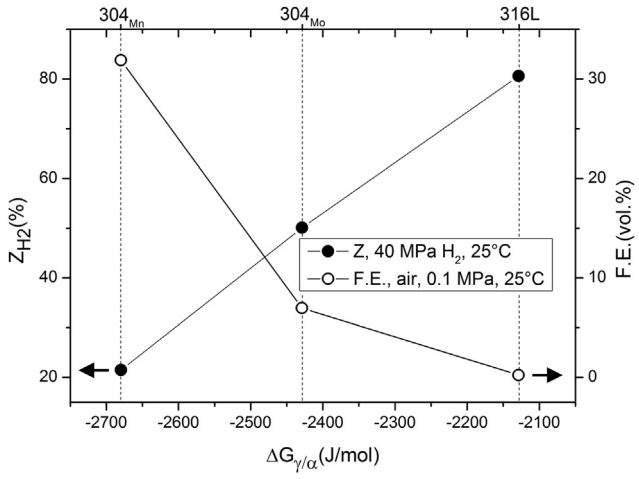

Fig. 1 – Reduction of area in hydrogen (Z_{H_2}) and the ferrite equivalent (F.E.) after tensile testing as a function of thermodynamic stability [26].

the differences on the $\gamma \rightarrow \alpha'$ transformed volumes can be attributed to the magnitude of the chemical driving force $\Delta G_{\gamma/\alpha}$ [30,26]. Similarly, a consistent correlation was found between the reduction of area (Z) and the calculated $\Delta G_{\gamma/\alpha}$. As shown in Fig. 1, the ductility response in hydrogen increases with the thermodynamic stability of the alloy [26]. These findings motivated us to use $\Delta G_{\gamma/\alpha}$ as a design parameter that is sensitive to the stability of the austenite phase.

$$\Delta G_{\gamma/\alpha} = G_{bcc} - G_{fcc} \quad (1)$$

3.2. *Thermodynamics-based criterion*

The preliminary results presented in Section 3.1 motivated us to use thermodynamic calculations to design HGE-resistant steels. The main idea was already introduced by the authors in [26] and refers to tailoring of the chemical composition in order to achieve a certain thermodynamic stability. In particular, a chemical driving force of $\Delta G_{\gamma/\alpha} = -2100$ [J/mol] was identified as a threshold value because appears to be the critical driving force of the f.c.c. → b.c.c. martensitic transformation at room temperature [41]. Moreover, this magnitude is also in accordance with the calculated value at 25 °C for the reference material 316L, which shows a high stability against martensite formation (Table 1 and Fig. 1). Therefore, the first requisite for the novel alloys is to feature a chemical driving force at 25 °C that is lower than the threshold value, *i.e.* $|\Delta G_{\gamma/\alpha}| \leq 2100$, to provide an austenite phase with a high stability.

Studies on the effect of alloying elements on HGE of austenitic steels as well as empirical developments of HGE-resistant alloys led to the selection of the elements C, Si, Mn, Cr and Ni due to their positive effect on reducing HGE susceptibility [17,26,42]. In addition, the element Cu was also incorporated into the alloy design because it stabilises the austenite at solution-annealing temperatures and also increases the mechanical stability against α'-martensite formation [43,39]. A compositional range was defined for every element of interest (Table 2). A combination of refractory elements was also introduced, with the element iron balancing the full composition. The maximum nickel content was restricted to 8 wt. % to improve cost-efficiency. After defining both elements and the range of interest, one thousand different chemical compositions were created, and the corresponding $\Delta G_{\gamma/\alpha}$ values were calculated according to Equation (1) [26]. The difference in Gibbs free energy at 298.15 K (25 °C) was calculated with the ThermoCalc® S software in combination with the TCFE6.2 database. Since the same chemical composition was assumed for the ferrite and austenite phases, the Gibbs energy of every phase was calculated by imposing a metastable state instead of a thermodynamic equilibrium. The use of metastable states has already been implemented in the calculation of stacking fault energies of austenitic steels by means of thermodynamic data [44,45]. The first selection of alloys was based on the criterion $|\Delta G_{\gamma/\alpha}| \leq 2100$, which reduced the number of candidates to 457 compositions. All remaining compositions were subsequently introduced into a Schaeffler diagram to account for non-equilibrium contributions [46]. Only those alloys lying in the fully austenitic field were selected, which reduced the number of candidates to 72. From this point onwards, the very last group of alloys was manually selected on the basis of a clear difference in both $\Delta G_{\gamma/\alpha}$ values and the chemical composition. Accordingly, the six alloys presented in Table 3 were selected for casting and production of tensile specimens. Actual chemical compositions and corresponding grain sizes resulting from the production route described in Section 2.1 are presented in Table 4.

3.3. *Tensile testing*

The results of the tensile tests in air and in a hydrogen atmosphere are presented in Table 5 as the average value of two tests *per* atmosphere together with the ferrite equivalent values measured after testing. With respect to the mechanical properties, both the yield and tensile strengths were not affected by the presence of hydrogen in any case. A relatively

Table 1 – Preliminary study on the thermodynamic stability of austenitic steels. Chemical compositions in mass-%, uniform elongation in air (A_{g-air}), ferrite equivalent (F.E.) and $\Delta G_{\gamma/\alpha}$ values calculated at room temperature with the TCFE6.2 database [26]. Equivalences on the nomenclature of the alloys: 304_{Mn} = 8, 304_{Mo} = 11-Mo and 316L = 12 in [26].

Alloy	C	Si	Mn	Cr	Ni	Mo	N	Cu	A_{g-air} (%)	F.E.$_{air}$ (vol.%)	$\Delta G_{\gamma/\alpha}$ (J/mol)
304_{Mn}	0.014	0.56	1.04	17.89	8.23	0.20	0.085	0.28	53	32	−2679
304_{Mo}	0.018	0.70	1.90	17.80	8.63	0.98	0.072	0.63	54	7	−2429
316L	0.012	0.83	1.43	17.13	12.24	2.46	0.057	0.35	52	0.2	−2128

Table 2 – Elements and ranges of interest for optimisation of the austenite stability by means of thermodynamic calculations. Values in mass- %.

Element	C	Si	Mn	Cr	Ni	Cu	Σ Refractory elements	Fe
Range	0.02–0.2	0.2–2.0	1.5–10.5	13–20.0	4.4–8.0	0.3–3.0	0.5–5.0	Bal.

high yield strength was observed in alloys 4, 5 and 6 due to the solid-solution-strengthening effect of interstitial carbon and the refractory metals as substitutional elements. Two different behaviours were observed for the ductility response. Whereas the elongation to rupture (A) and reduction of area (Z) were greatly lowered in hydrogen atmosphere for alloy 1 and 2, the same properties were not affected in the case of alloys 3 to 6. Interestingly, alloys 1 and 2 featured a higher chemical driving force for the martensitic transformation compared to the other four alloys (Table 3). Such a difference is clearly reflected by the amount of martensite that is formed after testing and which is represented by the ferrite equivalent values (Table 5). Accordingly, a higher driving force $\Delta G_{\gamma/\alpha}$ facilitates the $\gamma \rightarrow \alpha'$ transformation, which in the presence of hydrogen is detrimental for the macroscopic ductility of the material. Exemplary tensile curves for both atmospheres are shown in Fig. 2. The weak ductility response of alloys 1 and 2 is clearly visible, whereas alloys 3 to 6 show equivalent performances in air and hydrogen.

3.4. *Fracture surfaces and fractography*

The ductility response of the novel alloys is visualised in the macroscopic view of the necking areas and fracture surfaces in Fig. 3. A severe embrittlement effect in alloy 1 and 2 is evidenced by the lack of deformation. In contrast, the four most stable alloys (3–6) show very ductile behaviour with a typical cup-and-cone rupture in both atmospheres. In particular, alloy 3 exhibits a typical cup-and-cone rupture in hydrogen atmosphere, which shows no difference to the rupture in air. Fractography of alloy 3 in hydrogen atmosphere is presented in Fig. 4, in which three regions of interest were defined: (a) the border surface, (c) the centre of the fracture surface and (b) the area in between (a) and (c). Regions (a) and (b) appear as smooth surfaces with a shallow and elongated structure of dimples. Region (c) features an uneven surface with two main dimple sizes in which bigger and deeper dimples are surrounded by a "network" of much smaller and shallower dimples. Accordingly, the whole fracture surface exhibits a ductile failure without evidence of hydrogen-assisted fracture on the microscopic scale.

Fractographic analyses performed on alloys 4 to 6 showed a ductile failure in a hydrogen atmosphere with the dimple morphology varying from one alloy to the other. Cracks were found on the fracture surfaces of alloys 4 and 5 (Fig. 5). Such cracks developed perpendicularly to the fracture surface and have a greater length and lower intensity in alloy 4 than in alloy 5. The fracture surface of alloy 6 appears to be free of cracks (Fig. 5).

4. Discussion

The development of new HGE-resistant austenitic steels must take account not only of a particular chemical composition, but also the resulting microstructure, segregation effects, probable deformation mechanisms and even the production route of parts to allow for surface finishing [9,16,19–22]. Consideration of so many parameters in the design of HGE-resistant alloys is unfeasible. However, it is possible to define a design criterion that includes those parameters which have a higher impact on HGE. In this work, the stability of the austenite phase against the formation of strain-induced α'-martensite was employed as a key aspect [2–7,18]. This criterion was used on the premise that a fully stable austenite is necessary, but not sufficient to guarantee immunity against HGE [26,23]. Therefore, the criterion primarily refers to the development of stable alloys. These alloys also have to provide lower production costs and high HGE resistance. Whereas the cost efficiency was implemented by reducing the nickel and molybdenum contents, the HGE-resistant character was based on the selection of alloying elements and the

Table 3 – Alloy selection based on thermodynamic stability. Chemical compositions in mass- % and $\Delta G_{\gamma/\alpha}$ values calculated at 25 °C with the TCFE6.2 database. The AISI type 316L employed as reference material is included for comparison purposes.

Alloy	C	Si	Mn	Cr	Ni	Cu	Mo	Σ Refractory elements	$\Delta G_{\gamma/\alpha}$ [J/mol]
1	0.1	1	5.5	16.5	8	1.5	–	1	−1859.5
2	0.1	1	5.5	16.5	8	1.5	–	1	−1851.3
3	0.05	0.2	12	18	8	3	–	0	−691.7
4	0.2	2	10.5	13.7	8	3	–	2	−663.9
5	0.2	2	10.5	13.7	8	3	–	2	−653.3
6	0.2	2	10.5	13.7	8	3	–	5	−595.5
$316L_{ref.}$	0.012	0.83	1.43	17.1	12.5	0.35	2.46	2.46	−2128

Note: the difference between alloys 1 and 2, as well as 4 and 5, relies on the combination of refractory elements.

Table 4 – Chemical composition in mass- % of the novel alloys measured on tensile specimens after testing by optical emission spark spectrometry.

Alloy	C	Si	Mn	Cr	Ni	Cu	Σ Refractory elements	N	Grain size (μm ± 5)
1	0.093	1.05	5.53	16.73	7.76	1.55	0.99	0.034	60
2	0.083	1.08	5.57	16.84	7.78	1.56	1.01	0.029	80
3	0.042	0.22	11.75	18.05	7.56	3.14	0.06	0.032	50
4	0.172	2.10	10.19	13.37	7.90	3.20	1.71	0.058	95
5	0.175	2.12	10.14	13.63	7.92	3.21	1.95	0.059	85
6	0.170	2.05	10.23	13.74	7.88	3.05	4.75	0.029	45

Table 5 – Mechanical properties of the novel alloys: tensile tests performed at −50 °C in air at atmospheric pressure and in a 40 MPa hydrogen gas atmosphere with an initial strain rate of $5.5 \cdot 10^{-5}\ s^{-1}$. Ferrite equivalent values (F.E.) measured after tensile testing employing a FeritScope® MP30 device.

Alloy	$R_{p0.2}$ [MPa]		R_m [MPa]		A [%]		Z [%]		F.E. [vol.%]	
	H_2	Air	H_2	Air	H_2	Air	H_2	Air	H_2	Air
1	294	321	742	765	44	88	27	82	13	12
2	282	259	739	742	48	85	32	82	13	11
3	215	216	659	615	72	70	78	78	3.1	3
4	377	340	821	767	75	74	71	74	0.8	0.6
5	348	406	786	766	71	69	74	73	0.8	0.5
6	377	383	855	789	61	62	66	63	0.9	0.7
$316L_{ref.}$	316	298	783	727	81	73	75	80	8	2.4

corresponding compositional ranges. Accordingly, the HGE-resistant character of certain alloys will result from sufficient austenite stability and a fruitful interaction of the aforementioned parameters.

The stability of the austenite was thermodynamically evaluated as the difference in Gibbs free energy between the austenite and ferrite phases, which represents the available chemical driving force for the martensitic transformation (Equation (1)) [31]. A threshold value of $\Delta G_{\gamma/\alpha} = -2100$ [J/mol] was defined because it has been reported as the critical driving force [41] and it agrees with the calculated value for the reference 316L steel (Table 3). Therefore, the methodology described in Section 3.2 pointed to compositions that provide higher stability by means of a lower driving force. Or in practical terms: compositions that lead to $|\Delta G_{\gamma/\alpha}| \leq 2100$. Since the $\Delta G_{\gamma/\alpha}$ values are calculated by means of the ThermoCalc® software, there is virtually no limitation on the use of this method. Thus, novel compositions are created from the alloying elements contained in the thermodynamic database and the corresponding thermodynamic stability assessed by means of computational calculations. This criterion proved to be very sensitive to the martensitic transformation. The experimental results presented in Fig. 1 clearly show that the higher the driving force is, the higher is the volume that transforms into martensite upon deformation.

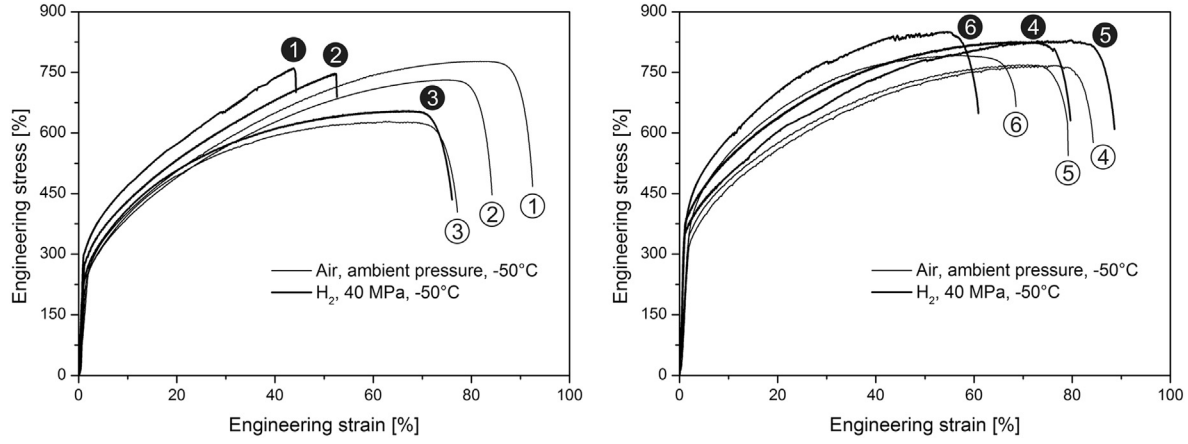

Fig. 2 – Engineering stress–strain curves of novel alloys obtained at −50 °C in air (white circles) and 40 MPa hydrogen gas (black circles).

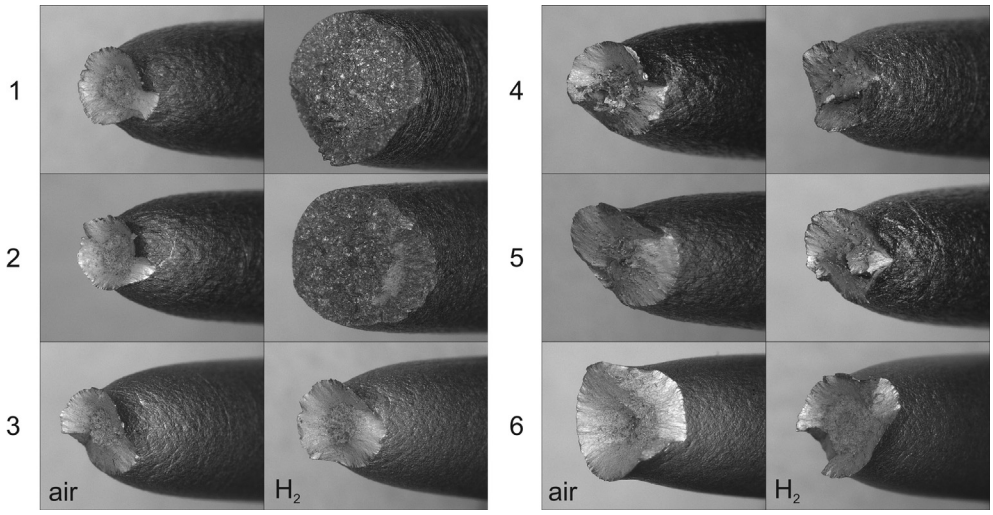

Fig. 3 – Macroscopic view of the necking area and fracture surface of novel alloys after testing at −50 °C; left: air at atmospheric pressure; right: 40 MPa hydrogen gas.

Table 3 presents the pointed chemical compositions of the novel alloys together with the corresponding $\Delta G_{\gamma/\alpha}$ values at 25 °C. Two groups can be identified in this table on the basis of a higher or lower driving force. The first group consists of alloys 1 and 2 with a relatively high value of around −1855 [J/mol], and the second group consists of alloys 3 to 6 with lower values ranging between −600 and −700 [J/mol]. Ferrite equivalent values measured after tensile testing clearly confirm the consistency of the thermodynamic approach (F.E. in Table 5). Specifically, the formation of strain-induced α'-martensite corresponds to the two levels of available driving forces. In this context, the ductility response was severely affected only in those cases where the formation of α' was favoured, *i.e.* in alloys 1 and 2 (Table 5). Although these two alloys were designed with a higher thermodynamic stability than the 316L reference material, the actual austenite stability of the

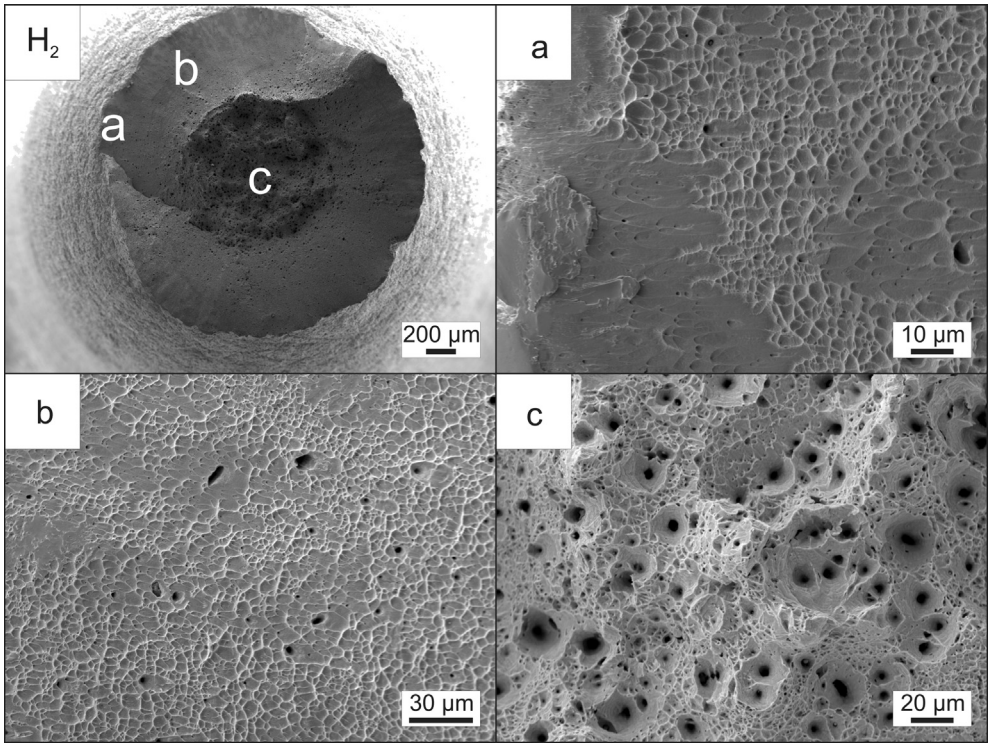

Fig. 4 – Fractography of alloy 3 tested at −50 °C in 40 MPa hydrogen gas atmosphere with an initial strain rate of $5.5 \cdot 10^{-5}$ s^{-1}.

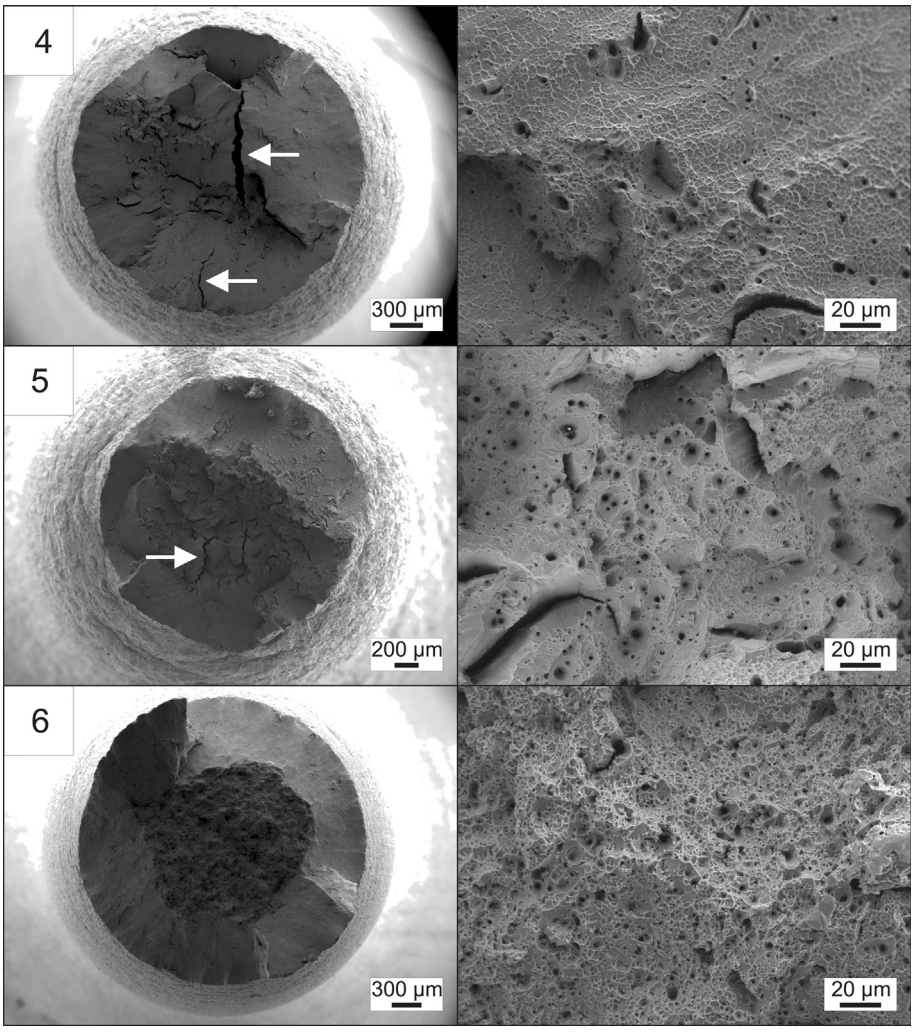

Fig. 5 – Fractography of alloy 4, 5 and 6 tested at −50 °C in 40 MPa hydrogen gas atmosphere with an initial strain rate of $5.5 \cdot 10^{-5}$ s^{-1}. Arrows indicate the presence of cracks in alloy 4 and 5 (left). Centre of the fracture surfaces (right).

austenitic phase was lower. Whereas alloys 1 and 2 reached a 13 vol.% ferrite equivalent after testing in hydrogen atmosphere, the 316L steel featured a value of 8 vol.% under the same testing conditions (Table 5). This discrepancy is attributed to the fact that the thermodynamic approach is based on the assumption of a fully homogeneous austenite with all alloying elements in a solid solution. This means that the effect of segregations, which can be quite different from one alloy to the next, are not considered in the thermodynamic calculations. Despite this limitation, the use of the $\Delta G_{\gamma/\alpha}$ criterion has been shown to be quite effective for alloy design. In particular, four of the six alloys have shown an equivalent behaviour in both atmospheres according to macroscopic observations and the tested mechanical properties (Fig. 3 and Table 5). Moreover, the high ductility in hydrogen is accompanied by a ductile failure, as presented in Figs. 4 and 5.

Although a high austenite stability against α'-martensite formation is not a sufficient condition to ensure immunity against HGE [23,25,26], no resistance to HGE is possible in the case of metastable alloys [5,18,26–28]. Experimental data collected by the authors of this work indicate that only those materials which experience a strain-induced α'-martensite formation lower than 10 vol.% feature a high resistance to HGE. This reference value is obtained *ex situ* through magnetic response measurements on tensile specimens tested to rupture, as described in Section 2.2. Exemplary cases are the reference material 316L, the novel alloys 3, 4, 5, 6 (Table 5), and the empirically developed 10Mn–8Ni–2.5Al steel presented in [17] with 1.1 vol.%. Accordingly, the 10 vol.% value can be set as an experimental threshold to qualify newly developed materials.

Among the novel materials developed by the current thermodynamic approach, alloy 3 appears to be the most promising candidate for hydrogen applications. The combination of a relatively simple chemical composition (Table 3), good mechanical properties (Table 5) and the complete absence of hydrogen-assisted fracture on the microscopic scale (Fig. 4) makes it a very attractive alternative material. Moreover, its behaviour suggests that the alloying with refractory elements, especially Mo, can be superseded if properties like corrosion resistance and hot strength are not required for a specific hydrogen application.

5. Summary

A thermodynamic approach was successfully implemented in the design of austenitic steels with a high resistance to hydrogen gas embrittlement (HGE). The method is based on the chemical driving force for the martensitic transformation as the representative parameter for the austenite stability. Computational calculations were used to define six novel compositions that featured a driving force lower than the critical value $\Delta G_{\gamma/\alpha} = -2100$ [J/mol]. Such alloys were produced in the laboratory and subjected to tensile testing in 40 MPa pure hydrogen gas at −50 °C together with a commercial AISI type 316L steel employed as a reference. Four of the six novel alloys showed a high resistance to HGE, as evidenced by the same elongation to rupture and reduction of area in hydrogen and air atmospheres. The implemented methodology led to the reduction of both time and experimental costs in comparison to empirical approaches. Moreover, a very high productivity was obtained from the thermodynamic approach in terms of the amount of alloys with a high resistance to HGE. To improve the cost-efficiency, the maximum nickel content was fixed to 8 wt.% and molybdenum was replaced by a combination of other refractory elements. Accordingly, a cost benefit is expected for these materials in comparison to the reference 316L steel.

Acknowledgement

The authors gratefully acknowledge financial support from the Bundesministerium für Wirtschaft und Technologie (BMWi) under contract number 0327802D. Tensile tests in hydrogen were performed at “The Welding Institute” (TWI, Cambridge, UK).

REFERENCES

[1] Birnbaum HK. Hydrogen embrittlementIn Encyclopedia of materials: science and technology; 2001. p. 3887–9.
[2] Eliezer D, Chakrapani DG, Altstetter CJ, Pugh EN. Influence of austenite stability on the hydrogen embrittlement and stress-corrosion cracking of stainless-steel. Met Trans A, Phys Metall Mater Sci 1979;10(7):935–41.
[3] Singh S, Altstetter C. Effects of hydrogen concentration on slow crack-growth in stainless-steels. Metall Trans A 1982;13(10):1799–808.
[4] Perng TP, Altstetter CJ. Comparison of hydrogen gas embrittlement of austenitic and ferritic stainless-steels. Met Trans A, Phys Metall Mater Sci 1987;18(1):123–34.
[5] Han G, He J, Fukuyama S, Yokogawa K. Effect of strain-induced martensite on hydrogen environment embrittlement of sensitized austenitic stainless steels at low temperatures. Acta Mater 1998;46(13):4559–70.
[6] Deimel P, Sattler E. Austenitic steels of different composition in liquid and gaseous hydrogen. Corros Sci 2008;(50):1598–607.
[7] Zhang L, Wen M, Imade M, Fukuyama S, Yokogawa K. Effect of nickel equivalent on hydrogen environment embrittlement of austenitic stainless steels at low temperatures, fracture of nano and engineering materials and structures. In: Proceedings of the 16th European Conference of Fracture.
[8] Marchi CS, Somerday BP, Tang X, Schiroky GH. Effects of alloy composition and strain hardening on tensile fracture of hydrogen-precharged type 316 stainless steels. Int J Hydrogen Energy 2008;33(2):889–904.
[9] Michler T, Naumann J. Hydrogen environment embrittlement of austenitic stainless steels at low temperatures. Int J Hydrogen Energy 2008;33(8):2111–22.
[10] Michler T, Yukhimchuk AA, Naumann J. Hydrogen environment embrittlement testing at low temperatures and high pressures. Corros Sci 2008;50(12):3519–26.
[11] Zhang L, Wen M, Imade M, Fukuyama S, Yokogawa K. Effect of nickel equivalent on hydrogen gas embrittlement of austenitic stainless steels based on type 316 at low temperatures. Acta Mater 2008;56(14):3414–21.
[12] Louthan MR, Caskey GR. Hydrogen transport and embrittlement in structural metals. Int J Hydrogen Energy 1976;1(3):291–305.
[13] Thompson AW. Structural materials use in a hydrogen energy economy. Int J Hydrogen Energy 1977;2:299–307.
[14] Nibur KA, Somerday BP, San Marchi C, Balch DK. Effects of strength and microstructure on hydrogen-assisted crack propagation in 22Cr–13Ni–5Mn stainless steel forgings. Metall Mater Trans A 2010;41(13):3348–57.
[15] West AJ, Louthan MR. Hydrogen effects on the tensile properties of 21-6-9 stainless steel. Metall Trans A 1982;13:2049–58.
[16] Nibur KA, Somerday BP, Balch DK, San Marchi C. The role of localized deformation in hydrogen-assisted crack propagation in 21Cr–6Ni–9Mn stainless steel. Acta Mater 2009;57(13):3795–809.
[17] Martin M, Weber S, Theisen W, Michler T, Naumann J. Development of a stable high-aluminum austenitic stainless steel for hydrogen applications. Int J Hydrogen Energy 2013;38(14):5989–6001.
[18] Perng TP, Altstetter CJ. Hydrogen effects in austenitic stainless-steels. Mat Sci Engi A 1990;129(1):99–107.
[19] Michler T, Lee Y, Gangloff RP, Naumann J. Influence of macro segregation on hydrogen environment embrittlement of sus 316L stainless steel. Int J Hydrogen Energy 2009;34(7):3201–9.
[20] Weber S, Martin M, Theisen W. Impact of heat treatment on the mechanical properties of aisi 304l austenitic stainless steel in high-pressure hydrogen gas. J Mat Sci 2012;47(16):6095–107.
[21] Martin M, Weber S, Izawa C, Wagner S, Pundt A, Theisen W. Influence of machining-induced martensite on hydrogen-assisted fracture of aisi type 304 austenitic stainless steel. Int J Hydrogen Energy 2011;36(17):11195–206.
[22] Nibur KA, Bahr DF, Somerday BP. Hydrogen effects on dislocation activity in austenitic stainless steel. Acta Mater 2006;54:2677–84.
[23] Michler T, San Marchi C, Naumann J, Weber S, Martin M. Hydrogen environment embrittlement of stable austenitic steels. Int J Hydrogen Energy 2012;37(21):16231–46.
[24] Kanezaki T, Narazaki C, Mine Y, Matsuoka S, Murakami Y. Effects of hydrogen on fatigue crack growth behavior of austenitic stainless steels. Int J Hydrogen Energy 2008;33(10):2604–19.
[25] Michler T, Naumann J. Hydrogen embrittlement of Cr–Mn–N-austenitic stainless steels. Int J Hydrogen Energy 2010;35(3):1485–92.
[26] Martin M, Weber S, Theisen W, Michler T, Naumann J. Effect of alloying elements on hydrogen environment embrittlement of AISI type 304 austenitic stainless steel. Int J Hydrogen Energy 2011;36(24):15888–98.

[27] Caskey GR. Hydrogen effects in stainless steel. In: Oriani RA, editor. Hydrogen degradation of ferrous alloys. Park Ridge and N.J: Noyes; 1985. p. 822–62.
[28] Mine Y, Narazaki C, Murakami K, Matsuoka S, Murakami Y. Hydrogen transport in solution-treated and pre-strained austenitic stainless steels and its role in hydrogen -enhanced fatigue growth. Int J Hydrogen Energy 2009;34:1097–107.
[29] Kaufman L, Hillert M. Thermodynamics of martensitic transformations. In: Olson GB, Owen WS, editors. Martensite. ASM International; 1992. p. 41–58.
[30] Tamura I, Wayman CM. Martensitic transformations and mechanical effects. In: Olson GB, Owen WS, editors. Martensite. ASM International; 1992. p. 227–42.
[31] Haidemenopoulos GN, Grujicic M, Olson GB, Cohen M. Thermodynamics-based alloy design criteria for austenite stabilization and transformation toughening in the Fe–Ni–Co system. J Alloys Comp 1995;220(1–2):142–7.
[32] McIntyre DR. Ranking materials for extreme sour gas service using the slow strain rate method. In: Raymond L, editor. Hydrogen embrittlement. ASTM; 1988. p. 178–89.
[33] Birnbaum HK, Sofronis P. Hydrogen-enhanced localized plasticity – a mechanism for hydrogen-related fracture. Mat Sci Engi A 1994;176(1–2):191–202.
[34] Standard practice for slow strain rate testing to evaluate the susceptibility of metallic materials to environmentally assisted cracking. ASTM International; 2006.
[35] Lecoester F, Chene J, Noel D. Hydrogen embrittlement of the Ni-base alloy 600 correlated with hydrogen transport by dislocations. Mat Sci Engi A 1999;262(1–2):173–83.
[36] Sun D, Han G, Vaodee S, Fukuyama S, Yokogawa K. Tensile behaviour of type 304 austenitic stainless steels in hydrogen atmosphere at low temperatures. Mat Sci Technol 2001;17(3):302–8.
[37] Louthan MR, Caskey GR, Donovan JA, Rawl DE. Hydrogen embrittlement of metals. Mat Sci Engi 1972;10(6):357–68.
[38] Talonen J, Aspegren P, Hanninen H. Comparison of different methods for measuring strain induced alpha-martensite content in austenitic steels. Mat Sci Technol 2004;20(12):1506–12.
[39] Nohara K, Ono Y, Ohashi N. Composition and grain size dependencies of strain-induced martensitic transformation in metastable austenitic stainless steels. ISIJ Int 1977;63(5):212–22.
[40] Ishida K. Calculation of the effect of alloying elements on the ms temperature in steels. J Alloys Comp 1995;(220):126–31.
[41] Borgenstam A, Hillert M. Driving force for fcc-bcc martensites in Fe-X alloys. Acta Mater 1997;45(5):2079–91.
[42] Weber S, Martin M, Theisen W. Lean-alloyed austenitic stainless steel with high resistance against hydrogen environment embrittlement. Mat Sci Engi A 2011;528(25–26):7688–95.
[43] Bain EC, Paxton HW. Alloying elements in steel. Am Soc for Metals 1966:100–42.
[44] Ishida K. Direct estimation of stacking fault energy by thermodynamic analysis. Phs Stat Sol (A) 1976;36:717–28.
[45] Miodownik AP. Calculation of stacking-fault energies in Fe–Ni–Cr alloys. CALPHAD-Comput Coupling Phase Diagrams Thermochem 1978;2(3):207–26.
[46] Schaeffler AL. Constitution diagram of stainless steel weld metal. Metal Progress 1949;1949(56):680.